Fabrication and Characterization of Mesoporous Co 3 O 4 Core/Mesoporous Silica Shell Nanocomposites

ARTICLE *in* THE JOURNAL OF PHYSICAL CHEMISTRY B · SEPTEMBER 2006

Impact Factor: 3.3 · DOI: 10.1021/jp0626465 · Source: PubMed

3 AUTHORS, INCLUDING:

Yongde Meng
Hanshan Normal University
8 PUBLICATIONS **92** CITATIONS
SEE PROFILE

Xiuling Jiao
Shandong University
132 PUBLICATIONS **3,603** CITATIONS
SEE PROFILE

Fabrication and Characterization of Mesoporous Co_3O_4 Core/Mesoporous Silica Shell Nanocomposites

Yongde Meng, Dairong Chen,* and Xiuling Jiao*

Department of Chemistry, Shandong University, Jinan 250100 P. R. China

Received: April 30, 2006; In Final Form: June 18, 2006

A mesoporous Co_3O_4 core/mesoporous silica shell composite with a variable shell thickness of 10−35 nm was fabricated by depositing silica on Co_3O_4 superlatticed particles. The Brunauer−Emmett−Teller (BET) surface area of the composite with a shell thickness of ca. 2.0 nm was 238.6 m^2/g, which varied with the shell thickness, and the most frequent pore size of the shell was ca. 2.0 nm. After the shell was eroded with hydrofluoric acid, mesoporous Co_3O_4 particles with a pore size of ca. 8.7 nm could be obtained, whose BET surface area was 86.4 m^2/g. It is proposed that in the formation of the composite the electropositive cetyltrimethylammonium bromide (CTAB) micelles were first adsorbed on the electronegative Co_3O_4 particle surface, which directed the formation of the mesoporous silica on the Co_3O_4 particle surface. Electrochemical measurements showed that the core/shell composites exhibited a higher discharge capacity compared with that of the bare Co_3O_4 particles.

1. Introduction

In the past decade, research on core/shell materials has become an active field because of their unique chemical and physical properties and potential applications in many areas.[1] The coating of shells on cores might alter the charge, function, and reaction of the cores and enhance their stability and compatibility,[2] which might provide a natural vehicle to obtain hybrid, multifunctional materials.[3] On the other hand, core/shell composites could present specific properties different from those of cores or shells.[4]

Since 1991, mesoporous silica has been extensively investigated for its potential applications in many fields such as catalytic supports, sensors, synthesis of nanostructured materials, optical hosts, and sorption media,[5] and there is an additional interesting research in the porous materials with a bimodal distribution having a distribution of both micropores or macropores and mesopores. However, being one of the most attractive fields, there has been a great deal of interest in creating a core/shell composite using mesoporous silica as the shell because the composite with a mesoporous shell has an unusually high activity/selectivity for many chemical reactions or a significant modification of the cores for some physical properties.[6] Many efforts have been devoted to fabricate new core/shell materials through modification of the components and structures of the core or shell. Recently, Shi's group fabricated uniform magnetic nanocomposite spheres with a magnetic core/mesoporous silica shell structure, and its drug storage capacity and in vitro release property were demonstrated.[7] Bouizi et al. reported that core/shell zeolite composites with a core and a shell of different structural types have both high separation and high adsorption capacity.[8] In this paper a novel core/shell nanostructure, composed of the mesoporous Co_3O_4 core and mesoporous silica shell, is introduced. A variable shell thickness could be obtained by adjusting the precursor concentration, and the formation mechanism of the core/shell structure was also investigated.

As an important magnetic P-type semiconductor, nanostructured Co_3O_4 displays high discharge capacity as the anode material in Li-ion rechargeable batteries and exhibits excellent sensitivity to hydrogen and alcohol because of its high surface area.[9] Many investigations focused on the promotion of its intrinsic properties by adjusting its structures and morphologies or substituting Co^{3+} cations with other metal ions or surface modification.[10] In the present work, mesoporous silica was coated on superlatticed Co_3O_4 particles to fabricate a mesoporous core/mesoporous shell composite. The objective of the present investigation was to create a composite built up of two single-phase mesoporous structures, which might exhibit some new properties or modify the physicochemical properties of the cores. On the basis of the investigation, a new mechanism for fabrication of core/shell composites was introduced, which might provide a new route for developing novel core/shell materials or mesoporous structures with a crystalline wall.

2. Experimental Section

2.1. Synthesis. All reagents were of analytical grade and were used as raw materials without further purification. The preparation of parent Co_3O_4 particles comprised of ordered aggregated nanocrystals followed our previous report.[11] In a typical synthesis, 0.5 g (1.7 mmol) of $Co(NO_3)_2 \cdot 6H_2O$ was dissolved in 8.0 mL of *n*-octanol to form a red solution at room temperature. The solution was added into 50 mL of *n*-octanol, heated to 180 °C, and refluxed at that temperature for 2 h, then separated by centrifugation to obtain a brown Co_3O_4 precipitate. To fabricate the core/shell composite, 0.1 g (0.4 mmol) of Co_3O_4 powder was ultrasonically dispersed in 200.0 mL of absolute ethanol to form a suspension. Then, 24.0 mL of ammonia solution (25 wt %) and 1.0 g of cetyltrimethylammonium bromide (CTAB) were added, followed by the dropping of 250.0 μL of tetraethoxysilane (TEOS) over 8 h under magnetic stirring. The molar ratio of $CH_3CH_2OH/H_2O/NH_3$/TEOS/CTAB in the system was 3434/1000/77.6/1.1/2.7. Then the solution reacted

* Corresponding authors. Phone: 086-0531-88364280. Fax: 086-0531-88364281. E-mail: cdr@sdu.edu.cn (D.C.); jiaoxl@sdu.edu.cn (X.J.).

10.1021/jp0626465 CCC: $33.50
Published on Web 07/18/2006

for a further 8 h under stirring, and the precipitate was separated by centrifugation, washed with absolute ethanol and water, heated to 500 °C with a heating rate of 1.0 °C/min, and held at that temperature for 6 h in a muffle oven.[6c] An amount of 0.2 g of core/shell composite was added into 50 mL of hydrochloric acid (50%, v/v) at the temperature of 50 °C under stirring for 4 h to dissolve the Co_3O_4 core and give the hollow sphere of mesoporous silica. On the other hand, after eroding the silica shell of the core/shell composite with 40 mL of 1:1 hydrofluoric acid at room temperature under stirring for 0.5 h, the mesoporous Co_3O_4 core could be obtained.

2.2. Characterization. X-ray diffraction (XRD) patterns were recorded using an X-ray diffractometer (Rigaku D/Max 2200PC) with a graphite monochromator and Cu Kα radiation (λ = 0.15418 nm). For estimating the crystallite size, the integral breadth of the (311) reflection with the Cu $K\alpha_1$ radiation is selected. To obtain the relative precise β-sample, the XRD pattern of micrometer Co_3O_4 crystalline particles obtained by the solid-state method was used as reference, in which the width of the peak from the size effect can be omitted, and the determined condition of the sample and the reference was held constant. On the basis of the observed integral breadth of the sample (B) and the reference (b), and the instrumental corrected curve, the integral breadth that resulted from the size effect (β-sample) was obtained, which is then applied to the calculation of the mean crystallite size using the Langford method.[12] In addition, the microstrain broadening was not taken into account during the calculation. A transmission electron microscope (TEM, model H-800) and a high-resolution transmission electron microscope (HR-TEM, JEOL-2010) were used to observe the morphology and microstructure of the samples. The infrared (IR) spectra were measured on a Fourier transform infrared spectrometer (Nicolet 5DX FTIR) using the KBr pellet technique. The zeta potential was measured using a Zeta meter (DXD-II). Nitrogen adsorption−desorption data were recorded on a Coulter 100cx at liquid nitrogen temperature ($T = -196$ °C). Electrochemical properties were studied by using a three-electrode cell with lithium metal as the counter and reference electrodes. The working electrode was prepared by mixing the active material (bare Co_3O_4, coated Co_3O_4 with varied shell thicknesses) with conductive material (carbon black) in a weight ratio of 17/5; after being dried at 100 °C for 4 h, the mixture was loaded into a bag made up of Ni net connected with 0.2 mm Ni wire as the down-lead and pressed with a pressure of 10 MPa for 0.2 h. The lithium foil pressed onto the Ni net was used as the reference and counter electrodes. The electrolyte was 1.0 mol·dm^{-3} $LiPF_6$ solution in ethylene carbonate (EC) and diethylene carbonate (DEC) with the volume ratio of 1/1. All the samples were calcined at 500 °C for 6 h to remove organic material before electrochemical measurement. Cyclic voltammetry measurement was carried out on a CHI660 electrochemical workstation, and the charge−discharge cycles were tested on a Land Series battery test system with a current density of 110 μA/cm^2 in the potential range of 0.01−3.0 V.

3. Results and Discussion

The wide-angle XRD patterns of core/shell particles and the parent Co_3O_4 particles (Figure 1a) showed that all the diffraction peaks could be indexed to the spinel Co_3O_4 with a lattice parameter of a = 0.8101 nm (JCPDS file no. 43-1003, a = 0.8084 nm), and the corresponding low-angle XRD (LA-XRD) pattern demonstrated an expanding peak at $2\theta \approx 1.3°$, indicating their superlattice nature (Figure 2a). After coating and calcination, all the characteristic diffraction peaks of spinel Co_3O_4 still remained (Figure 1b), showing the high thermal and chemical stabilities of Co_3O_4 nanocrystals. The decrease of the full width at half-maximum (fwhm) of the reflections demonstrated the increase of the Co_3O_4 nanocrystal size with calcination. On the basis of the calculation using the Langford method, the crystalline size of the parent Co_3O_4 particles was 20 nm, and that of the Co_3O_4 core in the composite was 29 nm, indicating the grain growth of the Co_3O_4 nanocrystals during the coating and calcination. After the Co_3O_4 cores were dissolved with hydrochloric acid, the LA-XRD pattern of the silica shell (Figure 2, inset) exhibited an expanding peak at $2\theta \approx 2.3°$, indicating its mesoporous nature. However, no peaks demonstrated the mesoporous structure of the Co_3O_4 cores after the silica shell was eroded by hydrofluoric acid, which might be due to the disorder and the wide pore size distribution of the mesopores as given by the following TEM and HR-TEM observations (Figure 4).

The IR spectrum of the parent Co_3O_4 particles (Figure 3a) shows two strong bands at ∼664 and ∼557 cm^{-1}, which are due to the ν (Co−O) modes;[13] the broad band at 3416 cm^{-1} and the peak at 1633 cm^{-1} correspond to the stretching and

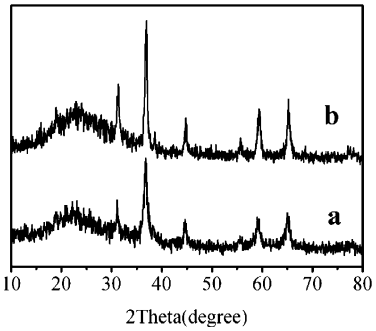

Figure 1. Wide-angle XRD patterns of Co_3O_4 particles (a) and the core/shell nanocomposite (b).

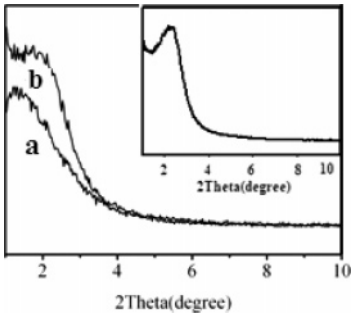

Figure 2. LA-XRD patterns of Co_3O_4 particles (a), core/shell nanocomposites (b), and the silica shell (inset).

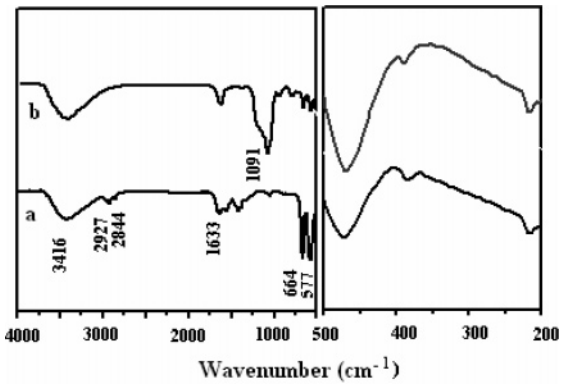

Figure 3. IR spectra of parent Co_3O_4 particles (a) and core/shell composite (b).

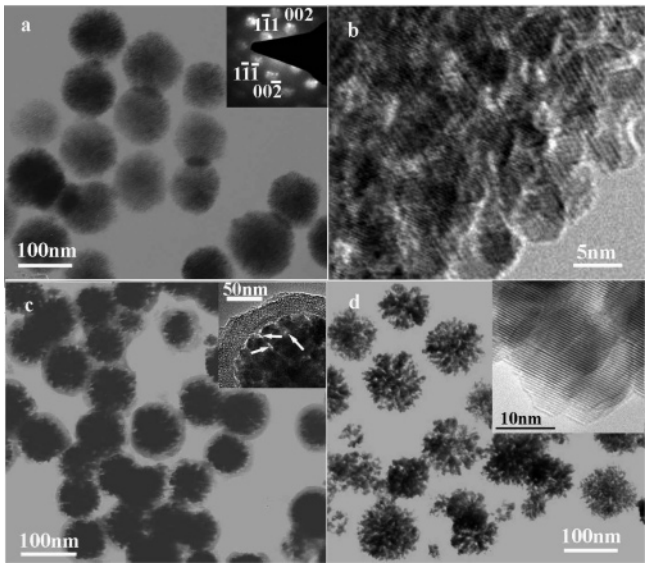

Figure 4. TEM images of Co_3O_4 particles (a), nanocomposite (c), Co_3O_4 core (d) (the shell is eroded by hydrofluoric acid), and the HR-TEM images of parent Co_3O_4 particles (b). The insets in (a), (c), and (d) are, respectively, the corresponding SAED pattern and the HR-TEM images.

bending modes of the surface hydroxyls and the hydroxyls of *n*-octanol.[11] However, the IR spectrum of the nanocomposite exhibits adsorptions at 1091 cm^{-1} (Figure 3b), which are assigned to the Si−O vibrations, and the bands at ca. 3400 and 1633 cm^{-1} are due to the adsorbed water. Because of the presence of the mesoporous SiO_2, the adsorptions of the Co−O vibrations significantly decreased. In addition, the peaks at 2927 and 2844 cm^{-1} attributed to the asymmetric and symmetric C−H stretching of the organics disappeared (Figure 3b), indicating the removal of organic materials upon calcination. The far-IR spectra of the composite shows no characteristic absorptions of Co−O−Si species, indicating that no chemical reaction between the Co_3O_4 core and SiO_2 shell occurred due to the low calcining temperature.[14]

TEM images of the core/shell nanocomposite showed the size of the parent Co_3O_4 particles ranging from 90 to 130 nm (Figure 4a), and the corresponding ED pattern (Figure 4a inset) revealed the oriented aggregation of the Co_3O_4 nanocrystals. Each Co_3O_4 particle consisted of the original Co_3O_4 nanocrystals with a size of ca. 6 nm (Figure 4b); the difference between the particle size from the XRD pattern, which was larger than the original nanocrystals but much smaller than the aggregates, and TEM observation was due to the oriented aggregation of the Co_3O_4 nanocrystals that composed the particle. Figure 4c clearly shows that each Co_3O_4 core was coated with a uniform silica shell, and the average thickness of the silica shell was ca. 20 nm. The HR-TEM image further indicated the formation of mesoporous Co_3O_4 core/mesoporous silica shell composite (Figure 4c inset); pores with a diameter of ca. 2.0 nm in the shell appeared in a disordered arrangement, and there were relatively larger pores with a size from 7.0 to 10.0 nm in the core (denoted by arrows in the inset of Figure 4c).

After calcination and erosion of the silica shell with 1:1 hydrofluoric acid, the mesoporous Co_3O_4 particles could be obtained (Figure 4d). The oriented aggregates of the Co_3O_4 nanocrystals gave rise to the mesopores, and the size of the Co_3O_4 nanocrystals increased to ca. 15 nm from the original nanocrystals with the size of ca. 6 nm. However, the crystalline size of the Co_3O_4 core different from that found by XRD analysis (the particle size based on XRD analysis was larger than that of the primary crystals that composed the aggregates but smaller than the size of the aggregates) is due to the ordered aggregation of the Co_3O_4 nanocrystals. As a comparison, the parent Co_3O_4 particles were also calcined at the same condition. Different from the core/shell composite, mesoporous Co_3O_4 particles could not be formed, and the nanocrystals significantly increased to ca. 60 nm from the original ca. 6 nm with the removal of the organics (Supporting Information, Figure S1). The result revealed that the silica coating depressed the grain growth of the Co_3O_4 nanocrystals during calcinations, which were easily carried out due to the high surface energy of the nanocrystals.[15] From the result, it could be concluded that the stability effect of the silica shell depressed the grain growth of the Co_3O_4 nanocrystals and resulted in the formation of the mesoporous Co_3O_4 core.[16a] Generally, the formation of the mesoporous materials was directed by the surfactant molecules, such as CTAB, P123, etc. Except for the typical fabrication of mesoporous materials using surfactant, there are a few reports on the fabrication of mesopores based on the aggregate and arrangement of the nanocrystals, in which the mesopores were formed from the interparticle spacing of the uniform nanoparticles.[16] However, the organic molecules coated on the nanoparticles are often necessary to lead to the arrangement in order, and the mesopores could be determined only after the removal of the organics. But the removal of the organics at a high temperature usually resulted in the growth of nanocrystals and the disappearance of mesopores. As to the present core/shell composite, the silica coating effectively depressed the grain growth of the Co_3O_4 nanocrystals during calcinations. As a result, a mesoporous Co_3O_4 core was formed upon calcination. The present work might provide a novel route to mesoporous materials without using surfactant. In addition, it can be seen that the Co_3O_4 particle size in the core/shell composite was much smaller than that of the parent Co_3O_4 particles after calcination. In previous reports, the preparation of metal or metal oxide nanocrystals by a liquid method has been extensively studied, and a series of nanocrystals and their oriented aggregates were successfully obtained. But the surface of the crystals were often stabilized with various organics to improve the dispersibility and uniform small size, and these organics sometimes destroyed the material's properties. To obtain surface-clean particles, calcination is a simple and effective route, but the calcinations often resulted in significant grain growth with the removal of the stabilizer. Therefore, this study might also provide a route to surface-clean nanocrystals.

The formation of the nanocomposite with a mesoporous silica shell and a mesoporous Co_3O_4 core has been further confirmed by the nitrogen adsorption−desorption isotherm (Figure 5). Two hysteresis loops appear in the relative pressure (p/p_o) range of 0.45−0.8 and 0.95−1 in the isotherm of the core/shell composite (Figure 5a), and one hysteresis loop appears in the relative pressure (p/p_o) range of 0.45−0.9 in the isotherm of the Co_3O_4 cores (Figure 5b). The hysteresis loop in the low relative pressure (p/p_o) range of 0.45−1 indicates the presence of mesopores in the core/shell composite. The hysteresis loop at $p/p_o = 0.95-1$ might result from the interparticle space formed by Co_3O_4 nanocrystal grains. The BET surface area of the nanocomposite is 238.6 m^2/g, and BJH analysis shows that the nanocomposite exhibits bimodal mesopore distributions, of which the most probable pore sizes are ca. 2.0 and ca. 8.8 nm, respectively, which was consistent with the HR-TEM images. After the silica shell was eroded by 1:1 hydrofluoric acid, the obtained mesoporous Co_3O_4 cores had a BET surface area of 86.4 m^2/g, and the most probable pore size was ca. 8.7 nm with

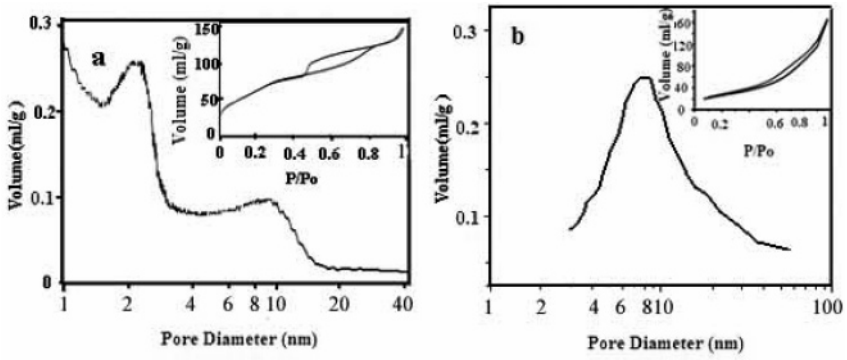

Figure 5. Calculated pore size distributions of the core/shell nanocomposite (a) and Co_3O_4 core (b). The insets are the corresponding N_2 adsorption−desorption isotherms, respectively.

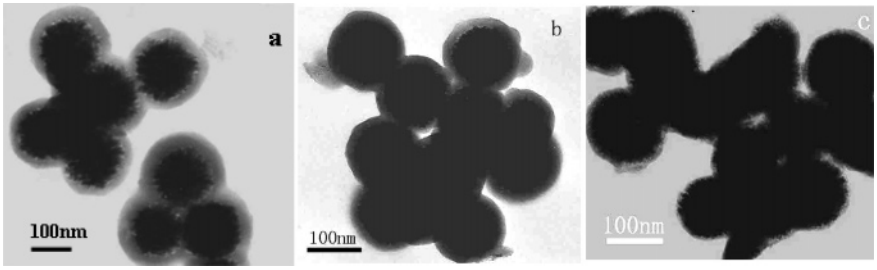

Figure 6. TEM images of core/shell nanocomposites prepared with different TEOS concentrations: (a) 9.0 mmol·dm^{-3}, (b) 5.0 mmol·dm^{-3}, and (c) 3.0 mmol·dm^{-3}.

TABLE 1: Properties of Core/Shell Composites with Different Shell Thicknesses

shell thickness (nm)	specific surface area BET (m^2/g)	most probable pore diameters of the shell and core from BJH_{ads} (nm)	specific pore vol (mL/g)
10	183.3	2.2 and 8.7	0.21
20	238.6	2.2 and 8.7	0.24
35	372.1	2.0 and 8.8	0.24

a wide pore size distribution, which originated from the aggregation of the Co_3O_4 nanocrystals.[17]

The formation of the mesoporous SiO_2 shell on the parent Co_3O_4 particles was carried out by hydrolysis and condensation of TEOS in a mixture of ethanol−water−ammonia at a pH value of 9.4. The dispersion of parent Co_3O_4 particles in the system is critical to the dispersibility of the core/shell composite. It was found that Co_3O_4 particles agglomerate on the surface of water but disperse in the presence of ethanol due to the chemisorbed *n*-octanol on the particle surface. The volume ratio of ethanol to water significantly affected the solvent polarity and the dispersibility of Co_3O_4 particles in the solvent. The suspension was stable, and the core/shell composite could be obtained when the volume ratio of ethanol to water was 200/18 in the mixture. When the volume ratio was decreased to 5/80, the Co_3O_4 particles agglomerated to form multinucleus core/shell composites (Supporting Information, Figure S2), and when the ratio was increased to 200/12 a slower deposit rate resulted. The thickness of the silica shell could be easily controlled by adjusting the TEOS concentration in the reaction system.[18] Experiments showed that the shell thickness could be varied from ∼10 to ∼35 nm by altering the TEOS concentration from 3 to 9 mmol·dm^{-3} (Figure 6); the corresponding BET surface area and BJH pore size are listed in Table 1.

In previous reports, the formation of the silica shell in the core/shell composite can be divided into two methods. Some surfaces can be directly coated with the silica due to the chemical affinity of these materials; however, other surfaces can only be coated with the help of stabilizer, surfactants, siliane coupling agents, or PVP coupling agent.[19] The following experiments were conducted to investigate the formation mechanism of the silica shell on parent Co_3O_4 particles. The result first confirms that Co_3O_4 particles cannot be directly coated with silica in the absence of CTAB surfactant, which reveals that CTAB is critical for forming the silica shell on the core. The zeta potential of the suspension (0.5 wt %) was tracked during the deposition of the mesoporous silica shell to probe the formation mechanism. According to Smoluchowski's equation, the zeta potential value of Co_3O_4 particles in the ethanol−water−ammonia mixture is −3.1 mV, indicating negative charging of the parent Co_3O_4 particles in the system. After the addition of the surfactant CTAB, in which its concentration (0.01 M) was well above the critical micelle concentration (cmc), the zeta potential value of Co_3O_4 increased up to −1.7 mV. It can be seen that although it is also negatively charged particles in the system, the negative charge density greatly decreases. It is reasonable to consider that this decrease results from the absorption of the positively charged CTAB micelles on the parent Co_3O_4 particle surface due to the electrostatic attraction. With further addition of TEOS into the mixture, all the Co_3O_4 particles could be coated with the silica shell because of the electrostatic attraction between the positively charged CTAB micelles and the negatively charged silicon species formed by hydrolysis and condensation. It is the positively charged CTAB micelles absorbed on the Co_3O_4 particle surface that directed the formation of the mesoporous silica shell. After the Co_3O_4 particles were coated with thin mesoporous silica shells, the zeta potential value of the composites decreased to −8.5 mV because of the coating of the negatively charged silicon species. Due to the larger negative charge density on the core/shell particle surface, the positively charged CTAB micelles continuously absorbed on

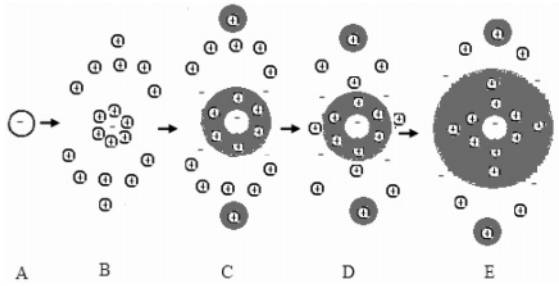

Figure 7. Proposed formation process of the core/shell composites: (A) the parent Co_3O_4 particle in the ethanol−water−ammonia mixture; (B) some CTAB micelles are adsorbed on the Co_3O_4 particle surface, others are free in the cosolvent; (C) formation of the silica shell and a few mesoporous silica particles; (D) CTAB micelles further adsorbed on the Co_3O_4 particle surface; (E) formation of a thicker silica shell.

the composite particle surface to increase the shell thickness. Except the core/shell composite formed in the system, there are a few mesoporous silica particles that existed in the product, which indicates that there are some free CTAB micelles in the solution but not absorbed on the particle surface. On the basis of this result, the experiment was carried out at a higher temperature to further confirm the formation mechanism of the shell by electrostatic attraction. It is found that many homogeneous mesoporous silica particles were accompanied with the core/shell particles while the injection of TEOS was conducted at a temperature of 40 °C. With the raising of the temperature, the hydrolysis and condensation significantly increased. It is to say that much more negatively charged silicon species were formed in a short period of time after the addition of TEOS. In this case, although the silicon species still preferred to absorb on the CTAB micelles absorbed Co_3O_4 particle surface due to the high charge density, much more silicon species still existed in the solution due to the high concentration, which assembled to form mesoporous silica particles using the free CTAB micelles as a template. A further experiment also revealed that shortening the dropping time of the TEOS resulted in more free mesoporous silica particles. On the basis of these experimental results, it can be concluded that the formation of the silica shell on the Co_3O_4 particles was due to the electrostatic attraction as illustrated in Figure 7.

Further experiments investigate the effect of the mesoporous silica shell on the electrochemical property of the nanostructured Co_3O_4 particle. The cyclic voltammograms (CVs) of electrodes made from the bare Co_3O_4 particles and core/shell composite with various shell thicknesses at a scan rate of 5.0 $mV \cdot s^{-1}$ at room temperature show that there is one broad redox peak in the potential range between 0.2 and 2.5 V, and the core/shell composite electrodes have a larger peak separation between the anodic and cathodic peaks compared with that of the bare Co_3O_4 electrode (Supporting Information, Figure S3).[20] Plateau currents can be observed at ca. 0.01 V in the curves of the core/shell composite, which might be caused by the slower Li^+ cations diffusion rate through the mesoporous silica layer.[21] With an increase of the shell thickness, the Li^+ cations diffusion rate through the mesoporous silica shell decreases. The curves of discharge capacity versus cycle number for the electrodes made from bare Co_3O_4 and composites indicate that all of the composite electrodes exhibit higher discharge capacity compared with that of the bare Co_3O_4 (Supporting Information, Figure S4). For the bare Co_3O_4 electrode, an initial discharge capacity of 658 mAh/g was obtained, while the initial discharge capacities of composite electrodes with different shell thicknesses were 821, 789, and 767 mAh/g, respectively. It is proposed that the significant increasing of the discharge capacity compared with that of the bare Co_3O_4 particles was due to the small size of the Co_3O_4 nanocrystals that composed the composite core. For composite electrodes with various shell thicknesses, the discharge capacity decreased with increasing shell thickness, which shows that the redox accessibility of Co_3O_4/Co is reduced with increasing shell thickness.[22]

4. Conclusions

The mesoporous Co_3O_4 core/mesoporous silica shell composite was successfully fabricated by directly depositing a silica shell on a Co_3O_4 superlatticed aggregate, and the thickness of the mesoporous silica layer could be controlled by adjusting the precursor concentration of TEOS. The most frequent pore sizes of the shell and core were ca. 2.0 and ca. 8.7 nm, respectively. IR and far-IR spectra indicate that there is no chemical reaction between the core and shell. The formation of the core/shell composite results from the electrostatic attraction between the parent Co_3O_4 particles, the CTAB micelles, the hydrolysis, and condensed silicon species. This synthetic strategy provides a novel route to mesoporous core/mesoporous shell composites or mesoporous structures with a crystalline wall or mesoporous silica hollow sphere. The core/shell composites exhibit higher discharge capacity than the uncoated Co_3O_4 particles. This improved performance might arise from the shells' inhibiting the crystal growth of Co_3O_4 nanocrystals and lead to a smaller size of Co_3O_4 nanocrystals in the core/shell composite than the bare Co_3O_4 particles.

Acknowledgment. This work was supported by the Program for New Century Excellent Talents in University, P. R. China.

Supporting Information Available: TEM images of the calcined Co_3O_4 particles and the multinucleus core/shell composite; CVs and cycle life of the electrode made by bare Co_3O_4 particles and composites with different shell thicknesses. This material is available free of charge via the Internet at http://pubs.acs.org.

References and Notes

(1) (a) Danek, M.; Jensen, K. F.; Murray, C. B.; Bawendi, M. G. *Chem. Mater.* **1996**, *8*, 173. (b) Dabbousi, B. O.; Rodriguez-Viejo, J.; Mikulec, F. V.; Heine, J. R.; Mattoussi, H.; Ober, R.; Jensen, K. F.; Bawendi, M. G. *J. Phys. Chem. B* **1997**, *101*, 9463. (c) Peng, X.; Schlamp, M. C.; Kadavanich, A. V.; Alivisatos, A. P. *J. Am. Chem. Soc.* **1997**, *119*, 7019. (d) Malik, M. A.; O'Brien, P.; Revaprasadu, N. *Chem. Mater.* **2002**, *14*, 2004. (e) Reiss, P.; Bleuse, J.; Pron, A. *Nano Lett.* **2002**, *2*, 781. (f) Hines, M. A.; Guyot-Sionnest, P. *J. Phys. Chem.* **1996**, *100*, 468. (g) Skumryev, V.; Stoyanov, S.; Zhang, Y.; Hadjipanayis, G.; Givord, D.; Nogues, J. *Nature* **2003**, *423*, 850. (h) Zeng, H.; Li, J.; Wang, Z. L.; Liu, J. P.; Sun, S. H. *Nano Lett.* **2004**, *4*, 187.

(2) (a) Ohmori, M.; Matijevic, E. *J. Colloid Interface Sci.* **1993**, *160*, 288. (b) Goia, D. V.; Matijevic, E. *New J. Chem.* **1998**, *22*, 1203. (c) Partch, R.; Brown, S. *J. Adhes.* **1998**, *67*, 259.

(3) Velikov, K. P.; Moroz, A.; van Blaaderen, A. *Appl. Phys. Lett.* **2002**, *80*, 49.

(4) (a) Kim, H.; Achermann, M.; Balet, L. P.; Hollingsworth, J. A.; Klimov, V. I. *J. Am. Chem. Soc.* **2005**, *127*, 544. (b) Grasset, F.; Labhsetwar, N.; Li, D.; Park, D. C.; Saito, N.; Haneda, H.; Cador, O.; Roisnel, T.; Mornet, S.; Duguet, E.; Portier, J.; Etourneau, J. *Langmuir* **2002**, *18*, 8209. (c) Mornet, S.; Grasset, F.; Portier, J.; Duguet, E. *Eur. Cells Mater.* **2002**, *3*, 110.

(5) (a) Kresge, C. T.; Leonowicz, M. E.; Roth, W. J.; Vartuli, J. C.; Beck, J. S. *Nature* **1992**, *359*, 710. (b) Bunker, B. C.; Rieke, P. C.; Tarasevich, B. J.; Campell, A. A.; Fryxell, G. E.; Graff, G. L.; Song, L.; Virden, J. W.; Mcvay, G. L. *Science* **1994**, *264*, 48. (c) Sayari, A. *Chem. Mater.* **1996**, *8*, 1840. (d) Corma, A. *Chem. Rev.* **1997**, *97*, 2373. (e) Yuliarto, B.; Zhou, H.; Yamada, T.; Honma, I.; Katsumura, Y.; Ichihara, M. *Anal. Chem.* **2004**, *76*, 6719. (f) Tura, C.; Coombs, N.; Dag, O. *Chem. Mater.* **2005**, *17*, 573. (g) Long, Y.; Xu, T.; Sun, Y.; Dong, W. *Langmuir* **1998**, *14*, 6173.

(6) (a) Büchel, G.; Unger, K. K.; Matsumoto, A.; Tsutsumi, K. *Adv. Mater*. **1998**, *10*, 1036. (b) Yu, K. M. K.; Thompsett, D.; Tsang, S. C. *Chem. Commun*. **2003**, *13*, 1522. (c) Lin, K.; Chen, L.; Prasad, M. R.; Cheng, C. *Adv. Mater*. **2004**, *16*, 1845. (d) Yu, J. S.; Yoon, S. B.; Lee, Y. J.; Yoon, K. B. *J. Phys. Chem. B* **2005**, *109*, 7040.

(7) Zhao, W.; Gu, J.; Zhang, L.; Chen, H.; Shi, J. *J. Am. Chem. Soc*. **2005**, *127*, 8916.

(8) Bouizi, Y.; Diaz, I.; Rouleau, L.; Valtchev, V. P. *Adv. Funct. Mater*. **2005**, *15*, 1955.

(9) (a) Li, W.; Xu, L.; Chen, J. *Adv. Funct. Mater*. **2005**, *15*, 851. (b) Wang, X.; Chen, X.; Gao, L.; Zheng, H.; Zhang, Z.; Qian, Y. *J. Phys. Chem. B* **2004**, *108*, 16401. (c) Epling, W. S.; Hoflund, G. B.; Weaver, J. F.; Tsubota, S.; Haruta, M. *J. Phys. Chem.* **1996**, *100*, 9929. (d) Takada, S.; Fujii, M.; Kohiki, S.; Babasaki, T.; Deguchi, H.; Mitome, M.; Oku, M. *Nano Lett.* **2001**, *1*, 379. (e) Wang, Y.; Yang, C.; Schmidt, W.; Spliethoff, B.; Bill, E.; Schüth, F. *Adv. Mater*. **2005**, *17*, 53.

(10) (a) Feng, J.; Zeng, H. C. *J. Phys. Chem. B* **2005**, *109*, 17113. (b) Natile, M. M.; Glisenti, A. *Chem. Mater.* **2003**, *15*, 2502. (c) Rondinone, A. J.; Samia, A. C. S.; Zhang, Z. J. *J. Phys. Chem. B* **1999**, *103*, 6876. (d) El-Shobaky, G. A.; Ghozza, A. M. *Mater. Lett.* **2004**, *58*, 699.

(11) He, T.; Chen, D.; Jiao, X. *Chem. Mater.* **2004**, *16*, 737.

(12) Audebrand, N.; Auffrédic, J.-P.; Loüer, D. *Chem. Mater*. **1998**, *10*, 2450.

(13) Pejova, B.; Isahi, A.; Najdoski, M.; Grozdanov, I. *Mater. Res. Bull*. **2001**, *36*, 161.

(14) Ocana, M.; Gonzalez-Elipe, A. R. *Colloids Surf., A* **1999**, *157*, 315.

(15) (a) Praserthdam, P.; Mekasuwandumrong, O.; Phungphadung, J.; Kanyanucharat, A.; Tanakulrungsank, W. *Cryst. Growth Des.* **2003**, *3*, 215. (b) Praserthdam, P.; Silveston, P. L.; Mekasuwandumrong, O.; Pavarajarn, V.; Phungphadung, J.; Somrang, P. *Cryst. Growth Des.* **2004**, *4*, 39. (c) Zhang, Q.; Clark, C. G., Jr.; Wang, M.; Remsen, E. E.; Wooley, K. L. *Nano Lett.* **2002**, *2*, 1051.

(16) (a) Yu, J. C.; Xu, A.; Zhang, L.; Song, R.; Wu, L. *J. Phys. Chem. B* **2004**, *108*, 64. (b) Sun, J.; Shan, Z.; Maschmeyer, T.; Moulijin, J. A.; Coppens, M. O. *Chem. Commun*. **2001**, 2670.

(17) Weibel, A.; Bouchet, R.; Boulc'h, F.; Knauth, P. *Chem. Mater*. **2005**, *17*, 2378.

(18) (a) Lu, Y.; McLellan, J.; Xia, Y. *Langmuir* **2004**, *20*, 3464. (b) Bahlawane, N.; Rivera, E. F.; Kohse-Höinghaus, K.; Brechling, A.; Kleineberg, U. *Appl. Catal., B* **2004**, *53*, 245.

(19) Graf, C.; Vossen, D. L. J.; Imhof, A.; van Blaaderen, A. *Langmuir* **2003**, *19*, 6693.

(20) He, T.; Chen, D.; Jiao, X.; Xu, Y.; Gu, Y. *Langmuir* **2004**, *20*, 8404.

(21) Zhang, Z.; Gong, Z.; Yang, Y. *J. Phys. Chem. B* **2004**, *108*, 17546.

(22) Suryanarayanan, V.; Nair, A. S.; Tom, R. T.; Pradeep, T. *J. Mater. Chem.* **2004**, *14*, 2661.